Synthetic Design of MLCT Excited States. Ligand-Substituted, Mono-2,2′-bipyridine Complexes of Ru(II)

Khaled R. Barqawi,[1a] Antoni Llobet,[1b] and Thomas J. Meyer*

Contribution from the Department of Chemistry, University of North Carolina, Chapel Hill, North Carolina 27514. *Received March 23, 1988*

Abstract: The role of the 2,2′-bipyridine ligand in metal to ligand charge transfer (MLCT) excited states and of the effect of substituent changes on that role has been investigated by spectroscopic and photochemical measurements on the series $[(tpm)Ru(4,4'-(X)_2-2,2'-bipyridine)(py)]^{2+}$ (X = $C(O)OC_2H_5$, C_6H_5, CH_3, NH_2, H; tpm is tris(1-pyrazolyl)methane).

For the metal to ligand charge transfer (MLCT) excited states of polypyridyl complexes of osmium(II) and ruthenium(II) the results of temperature-dependent lifetime,[2-17] resonance Raman,[18-24] and emission spectral fitting[6-8,21,25,26] have led to a relatively clear insight into excited-state structure and reactivity. It is becoming clearer as to what factors at the molecular level influence radiative and nonradiative decay rates, the pattern of low-lying excited states, structural differences between the ground and excited states, and the vibrational modes that participate in excited-state decay. One of the complexities that exists is the occurrence of contributions to excited-state decay and the appearance of ligand loss photochemistry from low-lying dd states.[3,5-17] Another issue in complexes containing more than one polypyridyl ligand has been whether the excited electron is localized on a single ligand or is delocalized over the available set.[18-24,27-37] These and related properties have been discussed in a recent review.[38]

With the insight gained it is possible to design and prepare families of related complexes for which MLCT excited-state properties can be varied systematically. In these complexes key excited-state properties vary with ground-state properties that are easily measurable such as Ru(III/II) reduction potentials and absorption band energies.[39] Although this is generally true for complexes of Os(II), it is not for Ru(II). For Ru(II) the presence of low-lying dd states can strongly influence excited-state lifetimes and stability. These states are not observable spectroscopically since the transitions are masked by higher intensity $d\pi \rightarrow \pi^*$ and ligand based $\pi \rightarrow \pi^*$ transitions. They are of lesser importance in complexes of Os(II) since there the splitting between the $d\pi$ and $d\sigma^*$ levels is ~30% higher. For Os(II) low-lying dd states are only encountered in complexes of low symmetry or where the energies of the MLCT states are relatively high.[38]

One of the challenges that remain in MLCT photochemistry is learning how to use synthetic modifications to manipulate the relative energies of MLCT and dd states. The goal is to "design out" the dd states since at worst they lead to photochemical degradation and, at best, they provide an additional channel for excited-state decay. Here, we report on the photochemical and photophysical properties of several complexes that contain a single, substituted, 2,2′-bipyridine ligand. The series is $[(tpm)Ru(4,4'-(X)_2-bpy)(py)](PF_6)_2$ (X = $C(O)OC_2H_5$, C_6H_5, CH_3, NH_2, H). Because of the simplifications in electronic structure offered

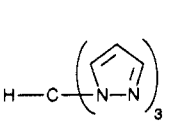

tpm

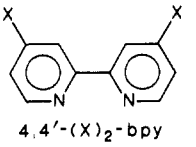

4,4′-(X)$_2$-bpy

by having a single polypyridyl ligand, the series offers a clear insight into the role of the chromophoric ligand in determining the spectroscopic and photochemical properties of MLCT excited states.

(1) (a) On sabbatical leave from Yarmouk University, Irbid-Jordan. (b) Fulbright "LaCaixa" fellow, Barcelona, Spain.
(2) Hager, G. D.; Crosby, G. A. *J. Am. Chem. Soc.* **1975**, *97*, 7031.
(3) Van Houten, J.; Watts, R. J. *Inorg. Chem.* **1978**, *17*, 3381.
(4) Allsop, S. R.; Cox, A.; Kemp, T. J.; Reed, W. J.; Carassiti, V.; Traverso, O. *J. Chem. Soc., Faraday Trans. 1* **1979**, 353.
(5) Durham, B.; Caspar, J. V.; Nagle, J. K.; Meyer, T. J. *J. Am. Chem. Soc.* **1982**, *104*, 4803.
(6) Caspar, J. V.; Meyer, T. J. *Inorg. Chem.* **1983**, *22*, 2444.
(7) Caspar, J. V.; Meyer, T. J. *J. Am. Chem. Soc.* **1983**, *105*, 5583.
(8) Allen, G. H.; White, R. P.; Rillema, D. P.; Meyer, T. J. *J. Am. Chem. Soc.* **1984**, *106*, 2613.
(9) Henderson, L. H.; Fronczek, F.; Cherry, W. R. *J. Am. Chem. Soc.* **1984**, *106*, 5876.
(10) Cherry, W. R.; Henderson, L. H. *Inorg. Chem.* **1984**, *23*, 983.
(11) Pinnick, D. V.; Durham, B. *Inorg. Chem.* **1984**, *23*, 3841.
(12) Juris, A.; Barigelletti, F.; Balzani, V.; Belser, P.; Von Zelewsky, A. *Inorg. Chem.* **1985**, *24*, 202.
(13) Wacholtz, W. M.; Auerbach, R. S.; Schmehl, R. H.; Ollino, M.; Cherry, W. R. *Inorg. Chem.* **1985**, *24*, 1758.
(14) Barigelletti, F.; Belser, P.; Von Zelewsky, A.; Juris, A.; Balzani, V. *J. Phys. Chem.* **1985**, *89*, 3680.
(15) Wacholtz, W. F.; Auerbach, R. A.; Schmehl, R. H. *Inorg. Chem.* **1986**, *25*, 227.
(16) Barigelletti, F.; Juris, A.; Balzani, V.; Belser, P.; Von Zelewsky, A. *J. Phys. Chem.* **1987**, *91*, 1095.
(17) Rillema, D. P.; Taghdiri, D. G.; Jones, D. S.; Keller, C. D.; Worl, L. A.; Meyer, T. J.; Levy, H. A. *Inorg. Chem.* **1987**, *26*, 578.
(18) Dallinger, R. F.; Woodruff, W. H. *J. Am. Chem. Soc.* **1979**, *101*, 4391.
(19) Foster, M.; Hester, R. E. *Chem. Phys. Lett.* **1981**, *81*, 42.
(20) Bradley, P. G.; Kress, B. A.; Hornberger, B. A.; Dallinger, R. F.; Woodruff, W. H. *J. Am. Chem. Soc.* **1981**, *103*, 7441.
(21) Casper, J. V.; Westmoreland, T. D.; Allen, G. H.; Bradley, P. G.; Meyer, T. J.; Woodruff, W. H. *J. Am. Chem. Soc.* **1984**, *106*, 3492.
(22) McClanahan, S. F.; Dallinger, R. F.; Moller, F. J.; Kincaid, J. R. *J. Am. Chem. Soc.* **1985**, *107*, 4853.
(23) Mabrouk, P. A.; Wrighton, M. S. *Inorg. Chem.* **1986**, *25*, 526.
(24) Poizat, O.; Sourisseau, C. *J. Phys. Chem.* **1984**, *88*, 3007.
(25) Kober, E. M.; Caspar, J. V.; Lumpkin, R. S.; Meyer, T. J. *J. Phys. Chem.* **1986**, *90*, 3723.
(26) Lumpkin, R. S.; Meyer, T. J. *J. Phys. Chem.* **1986**, *90*, 5307.
(27) Creutz, C.; Chou, M.; Netzel, T. L.; Okumura, M.; Sutin, N. *J. Am. Chem. Soc.* **1980**, *102*, 1309.
(28) Braterman, P. S.; Harriman, A.; Heath, G. A.; Yellowless, L. J. *J. Chem. Soc., Dalton Trans.* **1983**, 1801.
(29) Kober, E. M.; Sullivan, B. P.; Meyer, T. J. *Inorg. Chem.* **1984**, *23*, 2098.
(30) Kober, E. M.; Meyer, T. J. *Inorg. Chem.* **1984**, *23*, 3877.
(31) Braterman, P. S.; Heath, G. A.; Yellowless, L. J. *J. Chem. Soc., Dalton Trans.* **1985**, 1081.
(32) Milder, S. J.; Gold, Jon S.; Kliger, D. S. *J. Phys. Chem.* **1986**, *90*, 548.
(33) Ferguson, J.; Krausz, E. *Chem. Phys.* **1987**, *112*, 271.
(34) Ferguson, J.; Krausz, E. R.; Maeder, M. *J. Phys. Chem.* **1985**, *89*, 1852.
(35) Myrick, M. L.; Blakley, R. L.; DeArmond, M. K. *J. Am. Chem. Soc.* **1987**, *109*, 2841.
(36) Carlin, C. M.; DeArmond, M. K. *J. Am. Chem. Soc.* **1985**, *107*, 53.
(37) (a) Yersin, H.; Gallhuber, E. *J. Am. Chem. Soc.* **1984**, *106*, 6582. (b) Yersin, H.; Gallhuber, E.; Vogler, A.; Kunkley, H. *J. Am. Chem. Soc.* **1983**, *105*, 4155.
(38) Meyer, T. J. *Pure Appl. Chem.* **1986**, *58*, 1193.
(39) Kober, E. M.; Marshall, J. L.; Dressick, W. J.; Sullivan, B. P.; Caspar, J. V.; Meyer, T. J. *Inorg. Chem.* **1985**, *24*, 2755.

0002-7863/88/1510-7751$01.50/0

Experimental Section

Materials. All reagents were ACS grade and were used without further purification. Elemental analyses were performed by Galbraith Laboratories, Knoxville, TN.

Preparations. [(tpm)Ru(4,4'-$(X)_2$-bpy)(py)]$(PF_6)_2$ (X = $C(O)OC_2H_5$, C_6H_5, CH_3, NH_2, H). The complexes were prepared as PF_6^- salts by using the common procedure described below. In a typical experiment 50 mg of [(tpm)Ru(4,4'-$(X)_2$-bpy)(OH_2)]$(PF_6)_2$[40] were dissolved in 20 mL of a 0.1 M NH_4PF_6 ethanolic solution containing 3 mL of pyridine, and the resulting solution was heated at reflux for 6 h under argon. The solution was allowed to cool to room temperature and 5 mL of distilled water was added. The volume of the solution was reduced on a rotary evaporator until an orange crystalline solid began to form which was filtered in a Buchner funnel and washed with water (3 × 10 mL). The solid was recrystallized from a mixture of 1:5 water:acetone (v/v). Yield 90–95%. Anal. Calcd for (X = H) $C_{25}H_{23}N_9P_2F_{12}Ru$: C, 35.71; H, 2.74; N, 15.00. Found: C, 35.72; H, 2.78; N, 14.95. Anal. Calcd for (X = CH_3·0.75py) $C_{30.75}H_{30.75}N_{9.75}P_2F_{12}Ru$: C, 39.79; H, 3.32; N, 14.72. Found: C, 39.55; H, 3.63; N, 14.87. Anal. Calcd for (X = NH_2·2EtOH) $C_{29}H_{37}N_{11}O_2F_{12}Ru$: C, 36.17; H, 3.63; N, 16.00. Found: C, 36.59; H, 3.70; N, 16.14. Anal. Calcd for (X = $C(O)OC_2H_5$) $C_{31}H_{31}N_9O_4P_2F_{12}Ru$: C, 37.80; H, 3.15; N, 12.80. Found: C, 37.98; H, 3.30; N, 12.44. Anal. Calcd for (X = C_6H_5) $C_{37}H_{31}N_9P_2F_{12}Ru$: C, 44.75; H, 3.12; N, 12.70. Found: C, 46.24; H, 3.27; N, 11.97. Where present, independent evidence for the presence of the lattice solvent molecules was obtained by ^1H NMR.

Electrochemistry. Cyclic voltammetric measurements were carried out by using a PAR Model 173 potentiostat/galvanostat or a PAR 264A polarographic analyzer/stripping voltammeter. The cyclic voltammetric measurements utilized a Teflon sheathed glassy carbon disk (1.5-mm radius) working electrode, platinum wire auxiliary electrode, and a saturated sodium chloride calomel reference electrode (SSCE) in a one-compartment cell. UV grade acetonitrile was used as solvent and highly pure tetraethylammonium perchlorate (GFS Chemicals) as the supporting electrolyte. The $E_{1/2}$ values reported here were estimated from cyclic voltammetry as an average of the oxidative and reductive peak potentials ($E_{p,a} + E_{p,c}$)/2. UV–visible spectra were recorded by using a Hewlett-Packard Model 8451A UV–vis–diode array spectrophotometer with matched quartz 1-cm cells. The ^1H NMR spectra were recorded by using an IBM AC-200 spectrometer.

Emission Spectra and Quantum Yields. Corrected emission spectra were obtained in 4:1 EtOH/MeOH glasses at 77 K with a SLM Instruments, Inc., Model 8000 photon-counting fluorimeter. Emission quantum yields were determined in deoxygenated 4:1 EtOH/MeOH (v:v) solutions at 25 °C with samples of known optical density, compared to a standard sample of $[Ru(bpy)_3](PF_6)_2$ in acetonitrile solution for which (ϕ_{em} = 0.062).[7] Quantum yields were calculated by using eq 1[41,42] where ϕ_{std} is 0.062 at λ_{exc} = 436 nm. A is the solution absorbance at the

$$\phi_{em} = \phi_{std}\frac{A_{std}}{A_0}\frac{I_0}{I_{std}}\left(\frac{n}{n_{std}}\right)^2 \quad (1)$$

excitation wavelength, I is the emission intensity, and n is the index of refraction of the solvent.

Emission Spectral Fitting. Emission spectral fitting was carried out by using procedures and protocols that have been described in detail earlier.[21,25,43] A Vax 11/780 computer was used for the calculations. The experimental data were digitized and corrected to an abcissa linear in energy by using the method of Parker and Rees.[44] The form of the equation used in the fitting procedure is shown in eq 2, where I is the emitted light intensity at the energy $\bar{\nu}$ in wave numbers. In eq 2 v_M and

$$I(\bar{\Gamma}) = \sum_{v_M}\sum_{v_N}\{((E_{00} - v_M\hbar\omega_M - v_L\hbar\omega_L)/E_{00})^3(S_M^{v_M}/v_M!)(S_L^{v_L}/v_L!)\}$$
$$\{\exp[-4(\ln 2)((\bar{\nu} - E_{00} + v_M\hbar\omega_M + v_L\hbar\omega_L)/\Delta\bar{\nu}_{1/2})]^2\} \quad (2)$$

v_L are vibrational quantum numbers for the medium ($\hbar\omega_M$) and low ($\hbar\omega_L$) frequency acceptor modes. The summation was carried over five vibrational levels for the medium-frequency modes and over 15 vibrational levels for the low-frequency modes. Of the six parameters that appear in eq 2, (1) E_{00} is the energy (in cm^{-1}) of the v_M^*, $v_L^* = 0$ to v_M, $v_L = 0$ transition where v^* and v are the vibrational quantum numbers

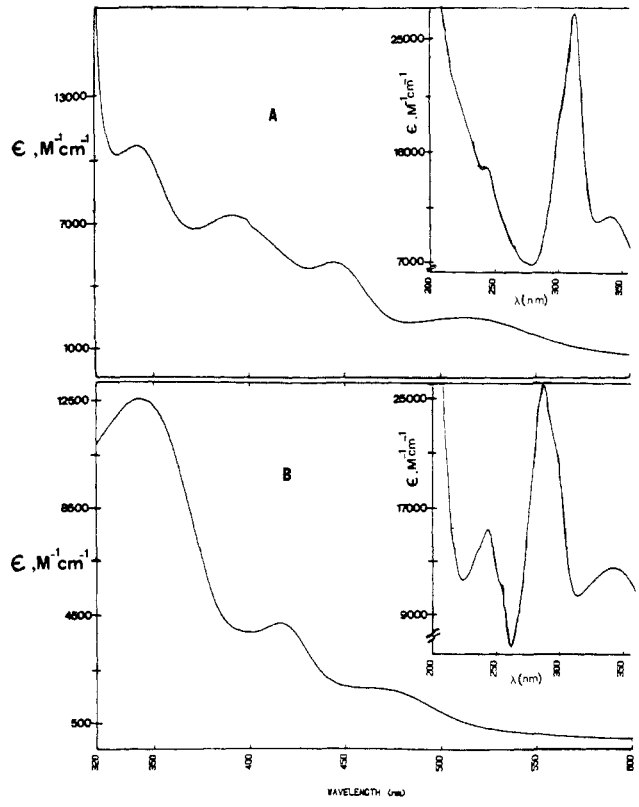

Figure 1. UV–vis absorption spectra in CH_3CN for the salts [(tpm)-Ru(4,4'-$(X)_2$-bpy)(py)]$(PF_6)_2$: (A) X = $C(O)OC_2H_5$ and (B) X = H.

for the excited and ground states, respectively, (2) S_M and S_L are the Huang-Rhys factors or electron–vibrational coupling constants for the medium- and low-frequency acceptor modes. S is related to the differences in equilibrium displacement between the ground and excited states (ΔQ_{eq}) and the reduced mass M for the participating normal modes by

$$S = \frac{1}{2}\left(\frac{M\omega}{\hbar}\right)(\Delta Q_{eq})^2 \quad (3)$$

(3) $\hbar\omega_M$ and $\hbar\omega_L$ are the quantum spacings for the medium- and low-frequency modes, and (4) $\Delta\bar{\nu}_{1/2}$ is the full width at half-maximum (fwhm) for the individual vibronic components that appear in the emission spectra. In the fits the six parameters were varied systematically except for $\hbar\omega_L$, which was held at 400 cm^{-1}, 350 cm^{-1} for the C_6H_5 derivative. In room temperature spectral fits $\hbar\omega_M$ and $\hbar\omega_L$ were held fixed at the 77 K values and the remaining parameters were varied systematically until a best fit was obtained.

Lifetime Measurements. Lifetime measurements were obtained by using a Molectron UV-400 nitrogen laser, coupled with a Molectron DL-200 tunable dye laser, as a pulsed light source (pulse width ~10 ns). Solutions were kept at 10^{-5}–10^{-4} M in order to prevent self-absorption or self-quenching and the precipitation of complex at low temperatures. They were prepared in 9 mm diameter Pyrex tubes and sealed under vacuum after being freeze–pump–thaw–degassed in at least four cycles. Because of the photosensitivity of the systems, the samples were prepared in the dark with excited-state measurements carried out under minimal photolysis conditions. The luminescence intensity at the wavelength of the emission maximum was monitored as a function of time following excitation with the use of an EMI Gencom Model RFI/S photomultiplier tube attached to a Bausch & Lomb 33-86-02 grating monochromator set at right angles to the excitation pulse. The photomultiplier output was fed to a Tektronix Model R7912 transient digitizer and then into a Digital PDP 11/34 minicomputer. Reported lifetimes are the averaged result of the analysis of 150 decay traces. Lifetimes were obtained by

(40) Doppelt, P.; Llobet, A.; Meyer, T. J. *Inorg. Chem.*, in press.
(41) Van Houten, J.; Watts, R. J. *J. Am. Chem. Soc.* **1976**, *98*, 4853.
(42) Guilbault, G. *Practical Fluorescence Theory, Methods and Techniques*; Marcel Dekker: New York, 1973; pp 11–14.
(43) Caspar, J. V. Ph.D. Thesis, The University of North Carolina, Chapel Hill, NC 1982.
(44) Parker, C. A.; Rees, W. T. *Analyst (London)* **1960**, *85*, 587.
(45) Bryant, G. M.; Fergusson, J. E. *Aust. J. Chem.* **1971**, *24*, 275.
(46) Felix, F.; Ferguson, J.; Gudel, H.; Ludi, A. *J. Am. Chem. Soc.* **1980**, *102*, 4096.
(47) (a) Kober, E. M.; Meyer, T. J. *Inorg. Chem.* **1982**, *21*, 3967. (b) Ferguson, J.; Herren, F. *Chem. Phys.* **1983**, *76*, 45.
(48) (a) Yersin, H.; Gallhuber, E.; Hensler, G. *Chem. Phys. Lett.* **1987**, *134*, 497. (b) Hensler, G.; Gallhuber, E.; Yersin, H. *Inorg. Chem.* **1987**, *26*, 1641. (c) Yersin, H.; Hensler, G.; Gallhuber, E. *Inorg. Chim. Acta* **1987**, *140*, 157.

Table I. Electrochemical (μ = 0.1 M) and Absorption Spectral Data in CH_3CN at 23 ± 2 °C

complex[a]	$E_{1/2}(Ru^{III/II})$[a]	$E_{1/2}(bpy^{0/-})$[b]	λ_{max} (ϵ)[c]	assignment
$[(tpm)Ru(4,4'\text{-}(C(O)OC_2H_5)_2\text{-}bpy)(py)]^{2+}$	1.27	−1.07,	514 (2380)	$d\pi \rightarrow \pi_1^*(bpy)$
		−1.63	446 (5070)	$d\pi \rightarrow \pi_1^*(bpy)$
			393 (7360)	$d\pi \rightarrow \pi_2^*(bpy)$
			342 (10 700)	$d\pi \rightarrow \pi^*(tpm)$
			314 (17 900)	$\pi \rightarrow \pi_1^*(bpy)$
				$\pi \rightarrow \pi^*(tpm)$
			246 (14 300)	$\pi \rightarrow \pi_2^*(bpy)$
$[(tpm)Ru(4,4'\text{-}(C_6H_5)_2\text{-}bpy)(py)]^{2+}$	1.12	−1.35	480 (3360)	$d\pi \rightarrow \pi_1^*(bpy)$
			428 (6870)	$d\pi \rightarrow \pi_1^*(bpy)$
			352 (16 500)	$d\pi \rightarrow \pi_2^*(bpy)$
				$d\pi \rightarrow \pi^*(tpm)$
			313 (35 000)	$\pi \rightarrow \pi_1^*(bpy)$
				$\pi \rightarrow \pi^*(tpm)$
			256 (39 800)	$\pi \rightarrow \pi_2^*(bpy)$
$[(tpm)Ru(4,4'\text{-}(H)_2\text{-}bpy)(py)]^{2+}$	1.15	−1.39	466 (1810)	$d\pi \rightarrow \pi_1^*(bpy)$
			416 (4220)	$d\pi \rightarrow \pi_1^*(bpy)$
			343 (12 500)	$d\pi \rightarrow \pi_2^*(bpy)$
				$d\pi \rightarrow \pi^*(tpm)$
			287 (25 800)	$\pi \rightarrow \pi_1^*(bpy)$
				$\pi \rightarrow \pi^*(tpm)$
			244 (15 200)	$\pi \rightarrow \pi_2^*(bpy)$
$[(tpm)Ru(4,4'\text{-}(CH_3)_2\text{-}bpy)(py)]^{2+}$	1.10	−1.51	462 (2000)	$d\pi \rightarrow \pi_1^*(bpy)$
			412 (4840)	$d\pi \rightarrow \pi_1^*(bpy)$
			348 (12 700)	$d\pi \rightarrow \pi_2^*(bpy)$
				$d\pi \rightarrow \pi^*(tpm)$
			288 (24 900)	$\pi \rightarrow \pi_1^*(bpy)$
				$\pi \rightarrow \pi^*(tpm)$
			247 (14 100)	$\pi \rightarrow \pi_2^*(bpy)$
$[(tpm)Ru(4,4'\text{-}(NH_2)_2\text{-}bpy)(py)]^{2+}$	0.87	−1.77	446 (2950)	$d\pi \rightarrow \pi_1^*(bpy)$
			374 (13 300)	$d\pi \rightarrow \pi_1^*(bpy)$
			337 (13 800)	$d\pi \rightarrow \pi_2^*(bpy)$
				$d\pi \rightarrow \pi^*(tpm)$
			303 (14 100)	$\pi \rightarrow \pi_1^*(bpy)$
				$\pi \rightarrow \pi^*(tpm)$
			247 (40 300)	$\pi \rightarrow \pi_2^*(bpy)$

[a] As PF_6^- salts. [b] Volts vs (SSCE) in CH_3CN solution with 0.1 M tetra-*n*-butylammonium perchlorate, $(TBA)ClO_4$, as supporting electrolyte. $E_{1/2}(Ru^{III/II})$ refers to the metal-based Ru(III)/Ru(II) couple and $E_{1/2}(bpy^{0/-})$ to bpy-based reductions. [c] λ in nm, ϵ values are in M^{-1} cm^{-1}.

weighted least-squares fit to a simple exponential decay. Variable temperature control was achieved with a modified Janis Instruments Model 6NDT "Varitemp" liquid nitrogen cryostat and a Lakeshore Cryotronics Model DRC 84C temperature controller.

Photochemical Quantum Yields. Quantum yields for the loss of pyridine (ϕ_p), e.g.

$$(tpm)Ru(bpy)(py)^{2+} + Cl^- \rightarrow (tpm)Ru(bpy)(Cl)^+ + py$$

were measured in acetonitrile containing 2 mM $[N(n\text{-}C_4H_9)]Cl$. The values reported here are relative to $[Ru(bpy)_3](PF_6)_2$ under the same conditions, where $\phi_p = 0.029$.[8] ϕ_p values were obtained by observing absorbance changes with time.

Results

Electrochemistry. In cyclic voltammograms of the tpm complexes in CH_3CN one reversible oxidation wave for the Ru(III/II) couple appears at positive potentials (relative to SSCE) to the solvent limit of ~2 V. Reductively, a single π^*(bpy)-based, reversible reduction wave appears to the solvent limit with the exception of the 4,4'-diester complex where a second, reversible reduction appears at −1.63 V vs (SSCE). Electrochemical data are summarized in Table I.

Absorption Spectra. Absorption spectra for the complexes $[(tpm)Ru(4,4'\text{-}(X)_2\text{-}bpy)(py)]^{2+}$ (X = $C(O)OC_2H_5$, H, NH_2) and $[(tpm)Ru(OH_2)_3]^{2+}$ are shown in Figures 1 and 2 and absorption spectral properties are summarized in Table I. The low-energy absorption bands for the bpy-containing complexes are $d\pi \rightarrow \pi^*$(bpy) in character.[45] The absorption band manifolds are broad and include contributions from a series of MLCT transitions and their vibronic components.[46-48]

Systematic trends do exist in the pattern of bands. For the diester complex (X = $C(O)OC_2H_5$), three separate MLCT absorption bands are observed. The energy difference between the lowest and highest is the ~6000 cm^{-1} energy separation between the two lowest π^*(bpy) levels π^*_1(bpy) and π^*_2(bpy).[45] The two lowest bands arise from transitions to π^*_1(bpy), $d\pi \rightarrow \pi_1^*$(bpy),

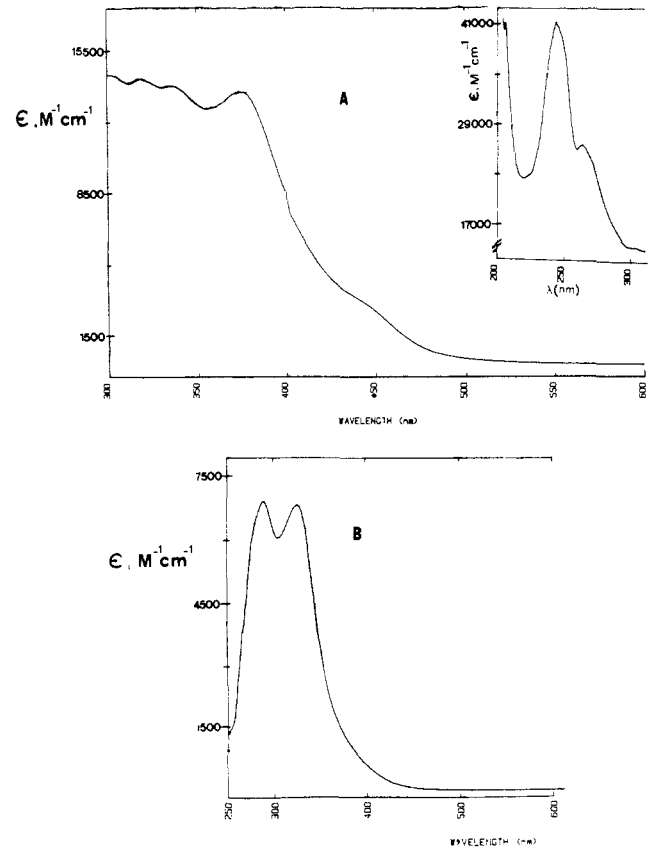

Figure 2. UV–vis absorption spectra in CH_3CN for the salts (A) $[(tpm)Ru(4,4'\text{-}(NH_2)_2\text{-}bpy)(py)](PF_6)_2$ and (B) $[(tpm)Ru(OH_2)_3](p\text{-}CH_3C_6H_4SO_3)_2$ in 0.1 M *p*-toluenesulfonic acid, pH 1.1.

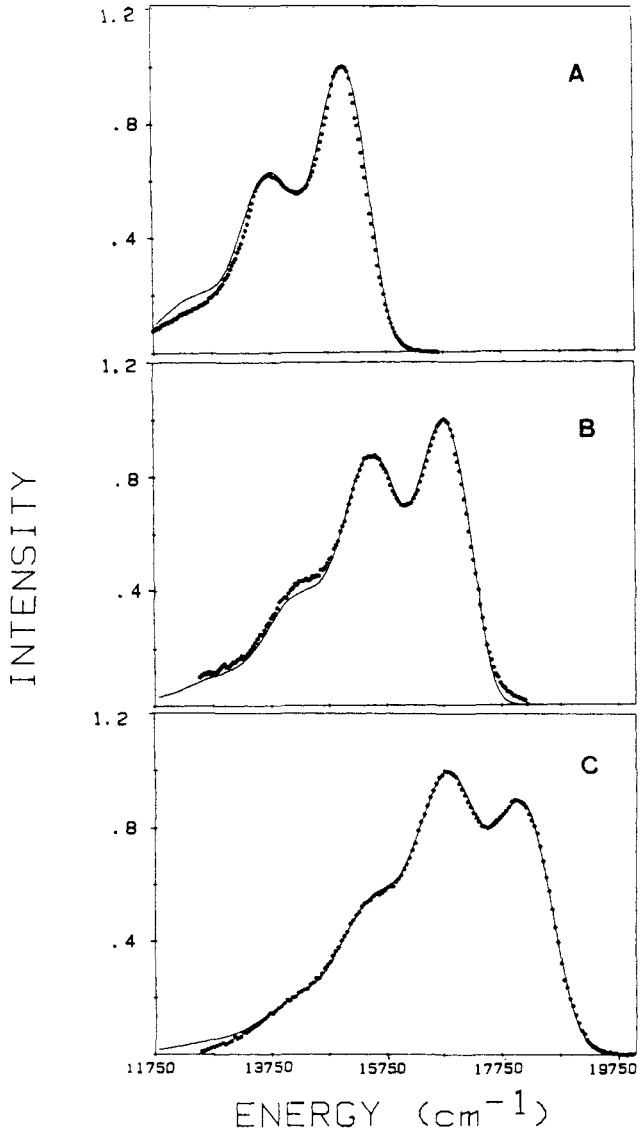

Figure 3. Emission spectra (*) at 77 K in 4:1 (v/v) EtOH/MeOH and fits (—) calculated by using the spectral parameters in Table III for the salts $[(tpm)Ru(4,4'\text{-}(X)_2\text{-}bpy)(py)](PF_6)_2$: (A) X = $C(O)OC_2H_5$, (B) X = H, and (C) X = NH_2.

and the third to $d\pi \rightarrow \pi_2^*$(bpy). The same pattern of bands is observed throughout the series with a shifting to higher energy occurring as the 4,4'-substituent on the bpy ligand becomes more electron donating. For $[(tpm)Ru(OH_2)_3]^{2+}$, $\pi-\pi^*$ and MLCT absorption bands appear at 290 and 326 nm, respectively. The presence of the tpm-based transitions further complicates the spectra leading, for example, to broad bands from 310–400 nm which include overlapping contributions from the transitions $d\pi \rightarrow \pi^*$(tpm), $d\pi \rightarrow \pi^*$(py), and $d\pi \rightarrow \pi_2^*$(bpy). At still higher energies the spectra are dominated by π(bpy) $\rightarrow \pi^*_1$(bpy) and π(tpm) $\rightarrow \pi^*$(tpm) transitions from 287–314 nm and by π(bpy) $\rightarrow \pi^*_2$(bpy) transitions from 244–256 nm.

Emission and Emission Spectral Fitting. In Figure 3 are shown emission spectra at 77 K for the salts $[(tpm)Ru(4,4'\text{-}(X)_2\text{-}bpy)(py)](PF_6)_2$ (X = $C(O)OC_2H_5$, H, NH_2) in 4:1 (v/v) EtOH/MeOH glasses. The emission manifold shifts to higher energy and the pattern of underlying vibronic contributions changes considerably as the 4,4'-substituent becomes more electron donating. From the results of resonance Raman[18-24] and low-temperature emission spectral fitting studies,[6,25,43] contributors to the emission spectral profile include the following: (1) 7 medium-frequency ν(polypyridyl) ring stretching modes, which appear in the spectra as an averaged mode of quantum spacing 1300–1400 cm^{-1}; (2) a series of low-frequency modes, including ν(M–L) metal–ligand stretching vibrations, which have an average

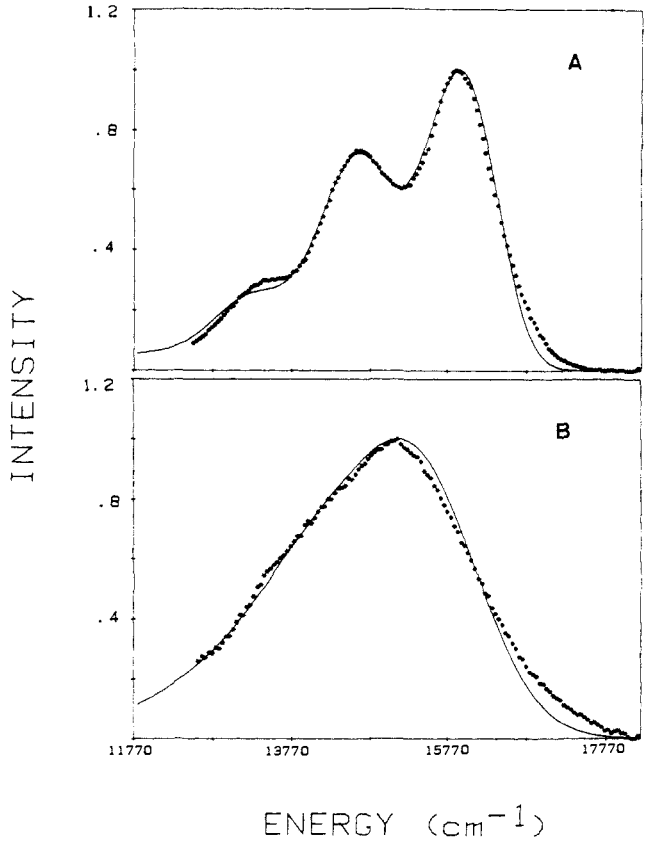

Figure 4. Emission spectra (*) and calculated fits (—) in 4:1 (v/v) EtOH/MeOH for $[(tpm)Ru(4,4'\text{-}(C_6H_5)_2\text{-}bpy)(py)](PF_6)_2$: (A) at 77 K and (B) at room temperature. The calculated fits at 77 K were obtained by using the spectral fitting parameters in Table III, which provided the basis for determining the fitting parameters at room temperature (see text).

quantum spacing of 300–400 cm^{-1} (the averaged low-frequency mode does not appear in the 77 K spectra but must be included in the spectral fits in order to obtain satisfactory agreement with the experimental spectra); and (3) solvent librational modes which are treated classically in the spectral fitting procedure.

The 77 K and room temperature spectra for $[(tpm)Ru(4,4'\text{-}(C_6H_5)_2\text{-}bpy)(py)](PF_6)_2$ are compared in Figure 4. At room temperature, a broad structureless emission is observed. The shift of the emission manifold to lower energy in fluid solution is a common observation for MLCT excited states.[49] Emission in the glass is at higher energy because the surrounding solvent dipoles are frozen in orientations appropriate to the ground state rather than the excited state.[26,50,51] At room temperature, significant emission is observed only for the complexes $[(tpm)Ru(4,4'\text{-}(X)_2\text{-}bpy)(py)]^{2+}$ (X = $C(O)OC_2H_5$, C_6H_5, H). Lifetimes at room temperature and 77 K, quantum yields for emission (ϕ_{em}) at room temperature, and quantum yields for loss of pyridine (ϕ_p)

(49) Wrighton, M.; Morse, D. L. *J. Am. Chem. Soc.* **1974**, *96*, 998.
(50) Kitamura, N.; Kim, H.; Kawanishi, Y.; Obata, R.; Tazuke, S. *J. Phys. Chem.* **1986**, *90*, 1488.
(51) Ferguson, J.; Krausz, E. *Chem. Phys. Lett.* **1986**, *127*, 551.
(52) Lumpkin, R. S.; Kober, E. M.; Meyer, T. J. *J. Phys. Chem.*, in press.
(53) (a) Bolleta, F.; Juris, A.; Maestri, M.; Sandrini, D. *Inorg. Chim. Acta* **1980**, *44*, L175. (b) Juris, A.; Barigelletti, F.; Balzani, V.; Belser, P.; Von Zelewsky, A. *Inorg. Chem.* **1983**, *22*, 3335. (c) Barigelletti, F.; Belser, P.; Von Zelewsky, A.; Juris, A.; Balzani, V. *J. Phys. Chem.* **1985**, *89*, 3680.
(54) Bensaason, R.; Salet, C.; Balzani, V. *C. R. Acad. Sci. Ser. B* **1979**, 41.
(55) Cook, M. J.; Lewis, A. P.; McAuliffe, G. S. G.; Skarda, V.; Thomson, A. J.; Glasper, J. L.; Robbins, D. J. *J. Chem. Soc., Perkin Trans. II* **1984**, 1293.
(56) Cook, M. J.; Lewis, A. P.; McAuliffe, G. S. G.; Skarda, V.; Thomson, A. J.; Glasper, J. L.; Robbins, D. J. *J. Chem. Soc., Perkin Trans. II* **1984**, 1303.
(57) Juris, A.; Belser, P.; Barigelletti, F.; Von Zelewsky, A.; Balzani, V. *Inorg. Chem.* **1986**, *25*, 256.

Table II. Excited-State Properties

complex	τ(77 K)[a] (μs)	τ(298 K)[a] (ns)	$\phi_{em} \times 10^3$[b]	ϕ_p[c]	$E^{o\prime}(Ru^{III/II*})$, V[d]	$E^{o\prime}(Ru^{II*/I})$, V[d]
$[(tpm)Ru(4,4'-(C(O)OC_2H_5)_2\text{-bpy})(py)]^{2+}$	2.36	334	6.5	<0.001	−0.51	0.71
$[(tpm)Ru(4,4'-(C_6H_5)_2\text{-bpy})(py)]^{2+}$	4.06	78	2.1		−0.84	0.61
$[(tpm)Ru(4,4'-(H)_2\text{-bpy})(py)]^{2+}$	4.21	(14)[e]	1.9	0.23	−0.88	0.64
$[(tpm)Ru(4,4'-(CH_3)_2\text{-bpy})(py)]^{2+}$	4.03	(3)[e]			−0.96	0.55
$[(tpm)Ru(4,4'-(NH_2)_2\text{-bpy})(py)]^{2+}$	6.27	(0.01)[e]		0.16	−1.33	0.43

[a] In 4:1 (v/v) EtOH/MeOH, ±2%. [b] Emission quantum yield at 23 ± 2 °C in 4:1 (v/v) EtOH/MeOH, ±15%. The excitation wavelength was 450 nm. [c] Quantum yield for loss of pyridine in CH_3CN containing 2 mM $[N(n\text{-}C_4H_9)_4]Cl$ at 23 ± 2 °C, ±15%. The excitation wavelength was 450 nm. [d] Excited-state reduction potentials calculated by using eq 4, $E_{1/2}$ values for the ground-state $Ru^{III/II}$ and $bpy^{0/-}$ couples in Table I in CH_3CN–0.1 M $[N(n\text{-}Bu)_4](ClO_4)$, and E_{oo}(298) in Table III obtained by emission spectral fitting in 4:1 (v/v) EtOH/MeOH. [e] Calculated by using eq 7 and the kinetic decay parameters in Table IV.

Table III. Emission Energies, Emission Spectral Fitting Parameters, and Franck–Condon Factors in 4:1 (v/v) EtOH/MeOH at 77 and 298 K

complex	T (K)	E_{em}[a] (nm)	E_{00}[b] (cm^{-1})	$\hbar\omega_M$[b] (cm^{-1})	S_M[b]	$\hbar\omega_L$[b] (cm^{-1})	S_L[b]	$\Delta\bar{\nu}_{1/2}$[b] (cm^{-1})	E_0[b] (cm^{-1})	$\Delta\bar{\nu}_{0,1/2}$[b] (cm^{-1})	ln (F(calcd))[c]
$[(tpm)Ru(4,4'-(C(O)OC_2H_5)_2\text{-bpy})(py)]^{2+}$	77K	665	15300	1375	0.74	400	1.1	670	15,050	1120	−20.4
	298K	725	14350	1375	0.56	400	1.4	1340	13,920	1810	−19.9
$[(tpm)Ru(4,4'-(C_6H_5)_2\text{-bpy})(py)]^{2+}$	77K	630	16210	1385	0.87	350	1.2	800	15,940	1140	−20.2
	298K	661	15800	1385	0.74	350	1.4	1500	15,390	1890	−20.0
$[(tpm)Ru(4,4'-(H)_2\text{-bpy})(py)]^{2+}$	77K	596	17120	1375	1.0	400	1.4	630	16,780	1220	−20.4
	298K	649	16370	1375	0.75	400	2.1	1230	15,720	1900	−20.6
$[(tpm)Ru(4,4'-(CH_3)_2\text{-bpy})(py)]^{2+}$	77K	590	17280	1365	1.0	400	1.4	650	16,890	1220	−20.9
	298K		(16580)[d]								
$[(tpm)Ru(4,4'-(NH_2)_2\text{-bpy})(py)]^{2+}$	77K	556	18460	1370	1.2	400	1.4	820	18,050	1350	−20.2
	298K		(17760)[d]								

[a] At 77 K the values are for the energy at the maximum of the first vibronic progression. [b] By emission spectral fitting, estimated errors are: ±5% for E_{00}, E_0, $\hbar\omega_M$, S_M, $\Delta\bar{\nu}_{1/2}$, and $\Delta\bar{\nu}_{0,1/2}$; ±10% for $\hbar\omega_L$ and S_L. [c] Calculated by using eq 5 and the results of emission spectral fitting. [d] Emission spectral fitting results are not available for the CH_3 and NH_2 derivatives at room temperature because they are weak emitters. Estimated values of E_{00} at 298 K were made from E_{00}(77 K) by the relationship, E_{00} (298 K) = E_{00}(77 K) + ΔE_s. The difference between E_{00}(298 K) and E_{00}(77 K), ΔE_s, arises because at 77 K the surrounding solvent dipoles are frozen in equilibrium orientations appropriate to the electronic distribution of the ground state while at 298 K the equilibrium solvent dipole orientations are appropriate to the electronic distribution of the excited state.[26,50,51] ΔE_s values were taken as the average of E_{00}(77 K) − E_{00}(298 K) = 700 cm^{-1} for the other three cases where emission could be observed at 298 K.

are all collected in Table II. Also included in Table II are estimates of reduction potentials for the excited states acting as oxidants,

$$(tpm)(bpy)Ru(py)^{2+*} + e \rightarrow (tpm)(bpy)Ru(py)^{+} \qquad E^{o\prime}(Ru^{2+*/+})$$

or reductants,

$$(tpm)(bpy)Ru(py)^{3+} + e \rightarrow (tpm)(tpy)Ru(py)^{2+*} \qquad E^{o\prime}(Ru^{3+/2+*})$$

The values were calculated (eq 4) from the ground-state potentials in Table II obtained in CH_3CN–0.1 M $[N(n\text{-}Bu)_4](ClO_4)$ and the E_{00} values in Table III in 4:1 (v/v) EtOH/MeOH obtained by emission spectral fitting. The values are only estimates since

$$E^{o\prime}(Ru^{2+*/+}) \sim E_{1/2}(bpy^{0/-}) + E_{00}(298) \qquad (4a)$$

$$E^{o\prime}(Ru^{3+/2+*}) \sim E_{1/2}(Ru^{III}/Ru^{II}) - E_{00}(298) \qquad (4b)$$

the $E_{1/2}$ and E_{00} values were obtained in different solvents. The E_{00} energies also include the solvent dipole reorganizational energy between the excited and ground states.

In addition to S_M, $\hbar\omega_M$, S_L, $\hbar\omega_L$, E_{00}, and $\Delta\bar{\nu}_{1/2}$, in Table III are summarized the results of emission spectral fitting at 77 and 298 K, the latter only for the $C(O)OC_2H_5$, C_6H_5, and H derivatives which emit appreciably at room temperature.

Table III also includes the spectral parameter E_0 and $\Delta\bar{\nu}_{0,1/2}$. E_0 is the band maximum for the first medium-frequency progression ($v_M^* = 0$ to $v_M = 0$) and $\Delta\bar{\nu}_{0,1/2}$ is the band width at half-maximum including contributions from both the solvent and the low-frequency mode treated classically.[25] The spectral fitting parameters can be used to calculate E_0 and the Franck–Condon (vibrational overlap) terms, F(calcd), the latter as in eq 5.

$$\ln [F(calcd)] = -(\ln [\hbar\omega_M E_0/(1000\ cm^{-1})^2])/2 - S_M - \gamma E_0/\hbar\omega_M + (\gamma + 1)^2(\Delta\bar{\nu}_{0,1/2}/\hbar\omega_M)^2/16 \ln 2 \qquad (5)$$

$$\gamma = \ln (E_0/S_M\hbar\omega_M) - 1 \qquad (5a)$$

The Franck–Condon terms are related to the rate constant for nonradiative decay by[25]

$$\ln (k_{nr} \times 1s) = \ln (\beta_0 \times 1s) + \ln [F(calcd)] \qquad (6)$$

In eq 6, β_0 is the vibrationally induced electronic coupling term. Equation 5 was derived for the case where nonradiative decay is dominated by a medium frequency acceptor mode or averaged mode ($\hbar\omega_M$) with additional contributions from a low-frequency mode and the solvent ($\Delta\bar{\nu}_{0,1/2}$) both treated classically. It is valid in the limit that $E_0 \gg \hbar\omega_M$ and $\hbar\omega_M \gg k_BT$.[25]

Temperature-Dependent Lifetimes. The results of temperature-dependent lifetime studies on polypyridyl complexes of Ru(II) have provided evidence for a series of temperature-dependent excited-state processes.[38] At low temperatures three closely spaced MLCT states exist which are largely triplet in character[2,4,48] with the upper two extensively mixed by spin–orbit coupling with low-lying singlets.[30,47] At temperatures near ambient, the three lowest lying MLCT states have significant Boltzman populations and behave kinetically as a single state, largely triplet in character, with decay properties dictated largely by the highest of the three states.

At higher temperatures additional temperature-dependent processes become important. They appear to have two origins: (1) thermal population and decay from an additional MLCT state, several hundred cm^{-1} higher in energy and having greater singlet character;[8,15,17,39,52] and (2) thermally activated surface crossing to low-lying dd states followed by rapid decay and commonly to loss of a ligand.

Lifetimes for the tpm complexes were obtained as a function of temperature in 4:1 (v/v) EtOH/MeOH. The data are available as supplementary material. The temperature dependences of the lifetimes could be satisfactorily fit to the expression in eq 7. The kinetic decay parameters so obtained are collected in Table IV.

$$[\tau_0(T)]^{-1} = k_1 + k^0 \exp[-\Delta E'/k_BT] \qquad (7)$$

In Figure 5 are shown plots of the inverse of the experimental lifetimes ($1/\tau_0$) vs $1/T$ in 4:1 (v/v) EtOH/MeOH for the NH_2

Table IV. Kinetic Decay Parameters from Lifetime Measurements in 4:1 (v/v) EtOH/MeOH

complex	T, K[a]	k_1,[b] $s^{-1} \times 10^{-6}$	k'^0,[b] $s^{-1} \times 10^{-15}$	$\Delta E'$,[b] cm^{-1}	k_{nr},[c] $s^{-1} \times 10^{-6}$	k_r,[c] $s^{-1} \times 10^{-4}$
$[(tpm)Ru(4,4'-(C(O)OC_2H_5)_2-bpy)(py)]^{2+}$	130–298	3.0 ± 0.5			3.0 ± 0.5	2.0 ± 0.4
$[(tpm)Ru(4,4'-(C_6H_5)_2-bpy)(py)]^{2+}$	130–280	0.95 ± 0.01	3.3 ± 2.2	4030 ± 180	0.92 ± 0.01	2.7 ± 0.5
$[(tpm)Ru(4,4'-(H)_2-bpy)(py)]^{2+}$	130–250	1.3 ± 0.03	0.13 ± 0.1	3000 ± 70	1.15 ± 0.04	
$[(tpm)Ru(4,4'-(CH_3)_2-bpy)(py)]^{2+}$	130–235	1.22 ± 0.04	1.8 ± 2	3200 ± 260	1.22 ± 0.04	
$[(tpm)Ru(4,4'-(NH_2)_2-bpy)(py)]^{2+}$	130–175	0.77 ± 0.33	11 ± 14	2450 ± 220	0.77 ± 0.33	

[a] Temperature range studied in the lifetime experiments. [b] From fits of the temperature-dependent lifetime data to eq 7. [c] Calculated from k_1 and ϕ_{em} values taken from Table II where $k_1 = k_{nr} + k_r$, $\phi_{em} = k_r\tau$, and $k_{nr} \sim 1/\tau$.

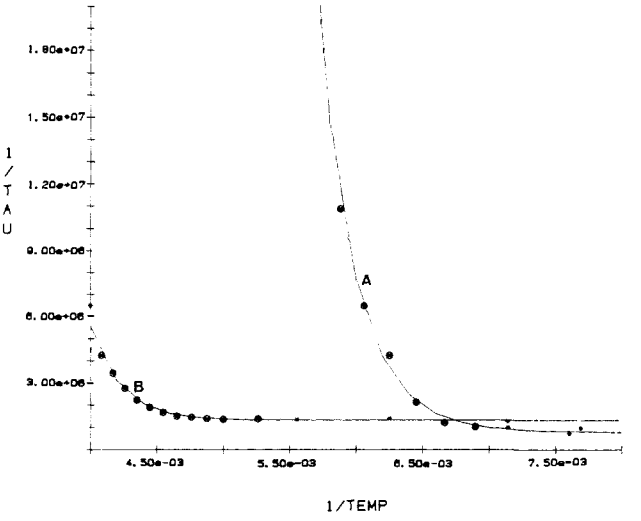

Figure 5. Comparison of experimental temperature-dependent lifetime data (*) in 4:1 (v/v) EtOH/MeOH with a computer-generated fit to the data by using eq 7 and the parameters in Table IV for $[(tpm)Ru(4,4'-(X)_2-bpy)(py)](PF_6)_2$: (A) X = NH_2 and (B) X = H.

and H derivatives. Also shown are calculated curves using the kinetic decay parameters in Table IV. A notable feature in the data is the absence of a temperature dependence for $[(tpm)Ru(4,4'-(C(O)OC_2H_5)_2-bpy)(py)]^{2+}$ and, at the same time, the absence of ligand loss photochemistry for this complex at room temperature (Table II).

In eq 7, k_1 is the sum of the radiative (k_r) and nonradiative (k_{nr}) decay rate constants for the emitting ^{3}MLCT state or states, and $\Delta E'$ and k'^0 are the activation energies and pre-exponential terms for the temperature-dependent term. The inclusion of a second temperature-dependent term as in eq 8 might be justified

$$[\tau_0(T)]^{-1} = k_1 + k_1'^0 \exp[-\Delta E_1'/k_BT] + k_2'^0 \exp[-\Delta E_2'/k_BT] \quad (8)$$

microscopically given the possible existence of contributions to nonradiative decay from both a higher MLCT state or states and a dd state.[4,39,53] It is not justified by the data alone.

Consistent with eq 7, the emission quantum yield (ϕ_{em}) is given by

$$\phi_{em} = \frac{k_r}{k_r + k_{nr} + k'^0 \exp[-\Delta E'/k_BT]} = k_r\tau_0 \quad (9)$$

which assumes that the efficiency of population of the emitting state(s) following excitation, η_{isc} in eq 10, is unity.[54,55] k_r and

$$\phi_{em} = \eta_{isc}k_r\tau_0 \quad (10)$$

k_{nr} can be calculated from the experimental values for ϕ_{em} and τ_0. The results of the calculations are also shown in Table IV for those cases where there is sufficient emission at room temperature to measure ϕ_{em} reliably.

Discussion

Previous studies have explored the effects of medium and chromophoric and nonchromophoric ligand variations on the photophysical properties of MLCT excited states.[6,8,10,12-15,17,22,23,25,56,57,63] In the current work we have been able to focus our attention on effects arising solely from substituent changes in the chromophoric ligand in a coordination environment free of multiple chromophoric ligand effects.

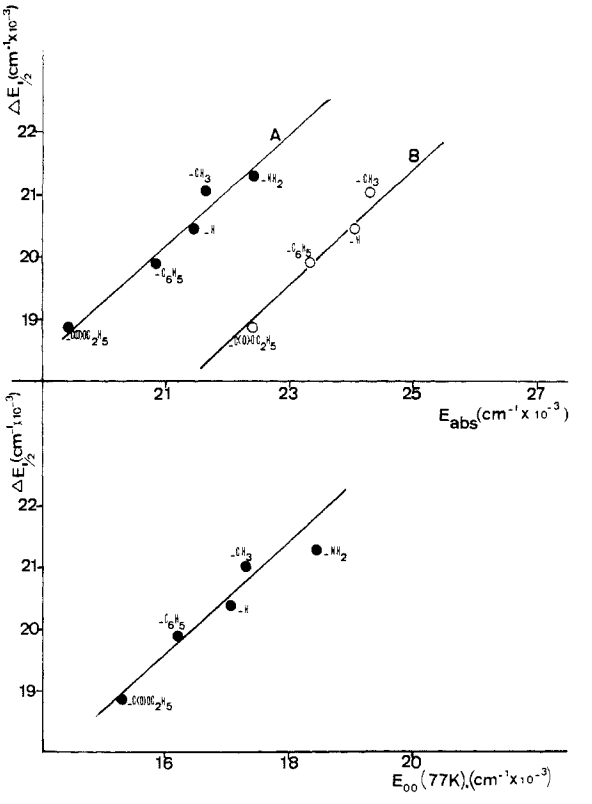

Figure 6. Plot of $\Delta E_{1/2} = E_{1/2}(Ru^{III/II}) - E_{1/2}(bpy^{0/-})$ in CH_3CN–0.1 M $[N(n\text{-}Bu)_4](PF_6)$ (Table I) vs E_{abs} (in CH_3CN) or E_{00} at 77 K in 4:1 (v/v) EtOH/MeOH by emission spectral fitting (Table III). The substituents at the 4,4' positions of the bpy ligands are indicated on the correlations. The absorption energies, E_{abs}, are for (A) the lower energy $d\pi \rightarrow \pi_1^*$(bpy) transition and (B) the higher energy $d\pi \rightarrow \pi_1^*$(bpy) transition (Table I). The higher energy $d\pi \rightarrow \pi_1^*$ band for X = NH_2 is masked in the spectrum.

Electronic Structure. It is a characteristic and expected feature of MLCT absorption and emission that linear correlations exist between ground-state reduction potentials and the energies of emission or absorption. For example, the difference in potentials between the metal-based oxidation and ligand-based reductions, $\Delta E_{1/2} = E_{1/2}(Ru^{III/II}) - E_{1/2}(bpy^{0/-})$, are energy quantities for the outer-sphere equivalent

$$[(tpm)Ru^{III}(bpy)(py)]^{3+} + [(tpm)Ru^{II}(bpy)^{\bullet-}(py)]^+ \rightarrow 2[(tpm)Ru^{II}(bpy)(py)]^{2+}$$

(58) Rillema, D. P.; Allen, G.; Meyer, T. J.; Conrad, D. *Inorg. Chem.* **1983**, *22*, 1617.
(59) Curtis, J. C.; Meyer, T. J. *Inorg. Chem.* **1982**, *21*, 1562.
(60) Eggleston, D. S.; Goldsby, K. A.; Hodgson, D. J.; Meyer, T. J. *Inorg. Chem.* **1985**, *24*, 4573.
(61) Ernst, S.; Kaim, W. *J. Am. Chem. Soc.* **1986**, *108*, 3578.
(62) Johnson, S.; Westmoreland, T. D.; Barqawi, K. R.; Meyer, T. J. *Inorg. Chem.*, in press.
(63) Vining, W. J.; Caspar, J. V.; Meyer, T. J. *Inorg. Chem.* **1985**, *89*, 1095.

of emission

$$[(tpm)Ru^{III}(bpy)^{\bullet-}(py)]^{2+*} \rightarrow [(tpm)Ru^{II}(bpy)(py)]^{2+} + h\nu$$

Plots of $\Delta E_{1/2}$ vs E_{00} (77 K) obtained by emission spectral fitting (Table III) and of $\Delta E_{1/2}$ vs the energies of the two $d\pi \rightarrow \pi_1^*$ absorption bands for the tpm complexes are shown in Figure 6. There are insufficient data to give statistical significance to the suggested linear correlations. However, they do support the assignment of the absorption and emission bands as MLCT or LMCT in nature and that the underlying electronic structure remains constant as the chromophoric ligand is varied.

The sense of the variations in $\Delta E_{1/2}$ and E_{abs} or E_{em} as the substituents are varied in 4,4′-$(X)_2$-bpy is understandable qualitatively. In passing from the electron-withdrawing $C(O)OC_2H_5$ to the electron-donating NH_2 groups, $E_{1/2}(Ru(III/II))$ decreases from 1.27 to 0.87 V while $E_{1/2}(bpy^{0/-})$ decreases from −1.07 to −1.77 V. The greater sensitivity of the π^*(bpy)-based reductions to substituent changes (−0.77 V compared to −0.40 V) is expected since the substituents are directly bonded to bpy. The influence on the Ru(III/II) potential is still notable given the ~6 Å distance separating the substituents from the metal. In an electronic sense the substituent effects are transmitted to the metal by a combination of effects. Oxidation state III is stabilized by enhanced σ donation and oxidation state II by $d\pi \rightarrow \pi^*$(bpy) back-bonding.

In terms of excited-state properties, the important point is that the energy gaps between the $(d\pi)^6$ ground and $(d\pi)^5(\pi^*)^1$ excited states *increase* for electron-donating substituents. This happens because the donating substituents increase the energy of the π^*(4,4′-$(X)_2$-bpy) acceptor orbitals to a greater degree than they do the $d\pi$(Ru) donor orbitals.

In contrast to our observations, both emission and absorption band energies have been observed to *decrease* as the electron-donating ability of the substituents increases in a series of mixed bpy complexes.[15,22,23,56] The two observations are actually consistent. In the multiple chelates both emission and low-energy absorption are dominated by MLCT transitions to the ligand with the lowest lying π^* levels. In an unsymmetrical complex containing both an electron rich ligand, bpy′, and bpy, the lowest energy MLCT states are localized on bpy. The ligand bpy′ is a "spectator" rather than a participant, e.g.

$$(bpy')_2Ru^{III}(bpy^{\bullet-})^{2+*} \rightarrow (bpy')_2Ru^{II}(bpy)^{2+}$$

As a spectator, its influence on the energy gap comes from the stabilization of the $(d\pi)^5$ core in the $(d\pi)^5(\pi^*)^1$ excited states by electronic donation. As bpy′ becomes a better donor, the energy gap is *decreased*. The substituent-induced increase in energy that we see can only occur in multiple chelates if the substituent changes are made at the acceptor ligand of the lowest MLCT excited state.

Emission Spectral Fitting, Excited-State Structure, Franck–Condon Factors. The results of the emission spectral fitting experiments (Table III) allow us to explore additional aspects of the role of the chromophoric ligand. Those new aspects are how substituent variations change the structures of the excited states and how the structural changes influence excited-state decay properties.

The first point to make about the data is that satisfactory spectral fits were obtained in all cases for a common pattern of acceptor vibrations. The successful utilization of averaged high-frequency, $\hbar\omega_M$ = 1365–1385 cm^{-1}, and low-frequency, $\hbar\omega_L$ = 350–400 cm^{-1}, modes in all cases points to a common pattern of acceptor vibrations which is relatively unperturbed by substituent changes at the 4,4′ positions.

Electronically, the ground and excited states differ by loss of an electron from the highest energy of the three $d\pi$ orbitals, $(d\pi_1)^2(d\pi_2)^2(d\pi_3)^2 \rightarrow (d\pi_1)^2(d\pi_2)^2(d\pi_3)^1(\pi_1^*)^1$. From X-ray crystal structures of coordinatively equivalent complexes of Ru(II) and Ru(III),[60,61] it is expected that changes in Ru–N bond lengths between the ground and excited states should be small at least for relatively symmetrical cases like these whose the central metal ion is surrounded by six N-based heterocyclic ligands. The small magnitudes of the S_L values in Table III suggest that they are.

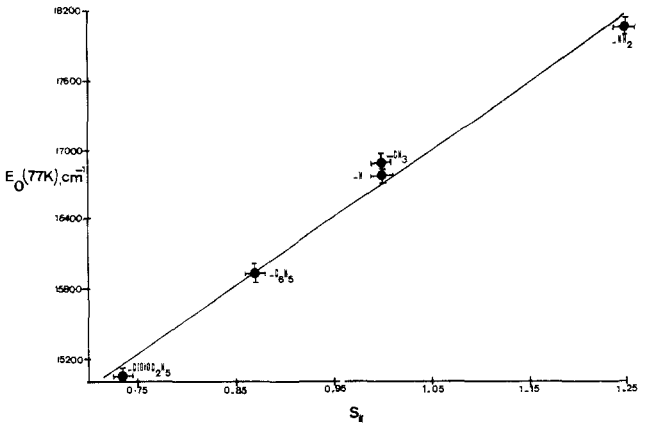

Figure 7. Plot of E_0 at 77 K in 4:1 (v/v) EtOH/MeOH vs S_M; data from Table III.

The S_L values include contributions to the emission spectral profile from low-energy vibrations, including those modes that are ν(Ru–N) in character.

For the medium frequency mode which is an average of contributions from 7 totally symmetrical ν(bpy) ring stretching modes, there are small but systematic increases in S_M as the energy gap increases. A plot of E_0 at 77 K vs S_M is shown in Figure 7. From the fundamental point of view, the more important energy quantity in such a correlation may be the true internal energy difference between the equilibrated states, ΔE_{ES}. Neglecting zero-point energy differences, ΔE_{ES} is given by $\Delta E_{ES} = E_0 - \lambda_0 - S_L\hbar\omega_L = E_{00} - \lambda_0$. The solvent dipole reorganizational energy, λ_0, is related to the full width at half-maximum by $(\Delta\bar{\nu}_{1/2})^2/16k_BT \ln 2$. From the data in Table III, $\Delta\bar{\nu}_{1/2}$ and $S_L\hbar\omega_L$ are essentially constant through the series and the same correlation is obtained with ΔE_{ES}, E_0, or E_{00}.

An increase of S_M with ΔE_{ES} is expected to exist. As the energy gap between the ground and excited states increases, the extent of ground- and excited-state mixing decreases. With less mixing the extent of charge transfer that occurs in the transition between states increases, which increases the distortion.[21,25,43]

It is possible to calculate the structural changes that occur at the bpy ligand between the excited and ground states from the S_M values. It follows from eq 3 that the average change in equilibrium displacement is given by $\Delta Q_e = (2\hbar S/M\omega)^{1/2}$. If it is assumed that the ring-based structural changes are shared equally over the C–N/C–C skeleton of the ring, the average change in local C–C or C–N bond lengths ($\Delta\bar{r}_e$) is given by[21]

$$|\Delta\bar{r}_e| = (2\hbar S_M/M_M\omega_M b)^{1/2} \quad (11)$$

In eq 11 M_M is the reduced mass for the medium-frequency mode and b is the total number of C–C plus C–N bonds. By using eq 11 it can be calculated that with M_M = 13,[21] $|\Delta\bar{r}_e|$ varies from 0.015 Å for X = $C(O)OC_2H_5$ to 0.019 Å for X = NH_2 at 77 K.

In the series of complexes $[(bpy)Os(L)_4]^{2+}$ and $[(phen)Os(L)_4]^{2+}$ (L = $^1/_2$bpy, $^1/_2$phen, CH_3CN, PR_3, ...) the MLCT energy gap can also be varied systematically, in this case by changing the nonchromophoric ligand, L.[25,43] S_M increases linearly with E_0 in that series as well. However, there is an interesting difference in the sensitivity of ΔQ_e (and Δr_e) to the energy gap for the two cases. When the energy gap is varied by changing the substituents on the chromophoric ligand in $[(tpm)Ru(4,4'\text{-}(X)_2\text{-bpy})(py)]^{2+}$, $(\partial S_M/\partial E_0) \sim 1.7 \times 10^{-4}$ cm. This corresponds to a change in $\Delta\bar{r}_e$ of 7.2×10^{-3} Å per 1000 cm^{-1} change in the energy gap. When the energy gap is varied by changing the nonchromophoric ligand in $[(bpy)Os(L)_4]^{2+}$, $(\partial S_M/\partial E_0) \sim 1.1 \times 10^{-4}$ cm.[25,43]

The greater sensitivity in the distortion at bpy to changes in X rather than L can be explained on electronic grounds. From perturbation theory neglecting overlap, the excited- and ground-state wave functions can be written to first order as

$$\Psi_{d\pi} = d\pi + \alpha\pi^* \quad (12a)$$

$$\Psi_{\pi^*} = \pi^* - \alpha d\pi \quad (12b)$$

where the mixing coefficient, α, is given by

$$\alpha = \frac{\langle \pi^* | \hat{H}' | d\pi \rangle}{E_{d\pi} - E_{\pi^*}} = \frac{H'}{\Delta E} \quad (13)$$

π^* and $d\pi$ are the unperturbed acceptor and donor wave functions and $E_{d\pi}$ and E_{π^*} the corresponding energies. $\hat{H}'$ is the operator that mixes $d\pi$ and π^*. It is assumed that overlap is negligible. When written as a linear combination of 2p N and C orbitals, π^* is given by

$$\pi^* = a_N 2p_N + a_1 2p_{C_1} + \ldots + a_4 2p_{C_4} + \ldots \quad (14)$$

The coefficients a are the appropriate weighting coefficients for the N atom, which is bonded to the metal, and for the various C atoms of the ring. Similarly, when metal ligand mixing between $d\pi$ and L is included, $d\pi$ can be written as

$$d\pi = d\pi^0 + \sum_j b_j \phi_j \quad (15)$$

The ϕ_j are wave functions for the low-lying π-acceptor orbitals on the ligands L and the b_j the corresponding mixing coefficients.

By using the expanded forms of the wave functions, the effect of changes in the π^*–$d\pi$ mixing induced by the 4,4′-bpy substituents, $\alpha(X)$, can be written as

$$\alpha(X) = \frac{\langle (a_N 2p_N + \ldots + a_4 2p_{C_4} + \ldots) | \hat{H}' | d\pi \rangle}{E_{d\pi} - E_{\pi^*}} = \frac{H'(X)}{\Delta E} \quad (15a)$$

For variations induced by L

$$\alpha(L) = \frac{\langle \pi^* | \hat{H}' | (d\pi^0 + \sum_j b_j \phi_j) \rangle}{E_{d\pi} - E_{\pi^*}} = \frac{H'(L)}{\Delta E} \quad (15b)$$

The extent of mixing of π^* into $d\pi$ is α^2 and the extent of $d\pi \rightarrow \pi^*$ charge transfer in the excited state is $1 - \alpha^2 = 1 - (H'/\Delta E)^2$. At least qualitatively, the extent of excited-state distortion and S_M are expected to increase as $1 - (H'/\Delta E)^2$ increases. S_M and by inference $1 - \alpha^2$ vary more dramatically with energy gap for changes in the bpy substituents than for changes in L. It follows that variations in X or L that lead to the same change in the energy gap cause a smaller change in $H'(X)$ than in $H'(L)$; that is $(\partial H'(X)/\partial \Delta E) < (\partial H'(L)/\partial \Delta E)$.

The basis for the smaller variation in $H'(X)$ can be seen in eq 15. In eq 15a overlap between $d\pi$ and π^*(bpy) is dominated by mixing of $d\pi$ with the 2p orbital on the bound N atom. The carbon atoms are spatially well separated from the metal ion and direct overlap with $d\pi$ is small. Variations in the substituents X at the remote 4,4′-positions most certainly affect E_{π^*} and ΔE.[62] However, they have a lesser effect on $d\pi$–$2p_N$ mixing than do variations in L. From eq 15b, variations in L influence $d\pi$ directly by back-bonding interactions. Variations in L affect $E_{d\pi}$ and the energy gap, but also the orbital composition of $d\pi$ directly. Variations in X are long distance in nature and transmitted through the ligand framework by a combination of σ and π effects.

Nonradiative Decay. All of the tpm complexes are relatively weak emitters with excited-state lifetimes that are largely controlled by nonradiative processes. In earlier work, variations in the nonchromophoric ligands,[6,25] the chromophoric ligands,[63] solvent,[7] ion-pairing,[64] and the glass-to-fluid transition[26] have all been used to demonstrate the existence of the linear relationship between ln k_{nr} and E_{em} predicted by the energy gap law. A more quantitative comparison with the predictions of radiationless decay theory has also been made by using emission spectral fitting to calculate Franck–Condon factors, eq 6.[25]

We have too few examples to attempt a quantitative analysis of the role of substituent changes at the bpy ligand on k_{nr} but there is a revealing feature in the data in Table II. In the earlier energy gap correlations, the appearance of linear relationships between ln k_{nr} and E_{em} or E_0 occurs because the term $-\gamma E_0/\hbar\omega_M$ in eq 5 accounts for >90% of the magnitude of the Franck–Condon factor and γ (= ln $(E_0/S\hbar\omega_M) - 1$) remains relatively constant as variations are made. Nonradiative decay is dominated by the term $-\gamma E_0/\hbar\omega_M$ because in the nonradiative decay process the major role as energy acceptor is played by the ν(bpy) ring-stretching modes. In the previous comparisons, γ remained relatively constant because the variations that led to an increase in E_0 increased S_M proportionately. The two changes roughly cancel, γ remains nearly constant, and ln k_{nr} varies linearly with E_0 ($-E_{em}$).

However, for substituent changes at the chromophoric ligand, $(\partial E_0/\partial S_M)$ is $\sim 5.8 \times 10^3$ cm^{-1} rather than $\sim 9.4 \times 10^3$ cm^{-1}. As E_0 increases, γ decreases. Since the two changes nearly compensate, the term $-\gamma E_0/\hbar\omega$ and the corresponding Franck–Condon factor remain nearly constant (Table III) even though significant variations occur in E_0. As shown by the data in Table II, when substituent changes are made at the 4,4′-positions in the bpy ligand, the simple energy gap law does not work. Even though variations occur in the energy gap, the Franck–Condon factor remains relatively constant.

By choosing appropriate nonchromophoric ligands in [(bpy)-Os(L)$_4$]$^{2+}$ it is possible to build in a high-energy gap and a long lifetime.[25,39] The lengthened lifetime is necessarily at the expense of a loss in low energy visible light absorptivity if the energy gap is large. When variations are made in the 4,4′-bpy substituents, a lowered energy gap increases k_{nr} but to a lesser degree and the loss in lifetime is far less. The enhanced lifetime is a consequence of the lowered dependence of k_{nr} on energy gap for the emitting MLCT state and, as discussed in the next section, the absence of a low-lying dd state.

An additional point that we had hoped to explore in the present study was the role of substituent effects on the electronic coupling term β_0

$$(\beta_0) = h^2\omega_k(\pi/2)^{1/2}/(1000 \text{ cm}^{-1})\left\langle \Psi_{ES}\left|\frac{\partial}{\partial Q_k}\right|\Psi_{GS}\right\rangle^2 \quad (16)$$

In eq 16 Ψ_{ES} and Ψ_{GS} are the electronic wave functions for the excited and ground states and ω_k and Q_k are the angular frequency and coordinates of the "promoting mode". The term $\partial/\partial Q_k$ is a Born–Oppenheimer operator for that mode or modes which have the appropriate symmetry properties to mix the two states. Given the electronic structure of the initial, $(d\pi_1)^2(d\pi_2)^2(d\pi_3)^1(\pi_1^*)^1$, and final, $(d\pi_1)^2(d\pi_2)^2(d\pi_3)^2$, states, the vibrationally induced electronic coupling integral is given by

$$\left\langle \Psi_{ES}\left|\frac{\partial}{\partial Q}\right|\Psi_{GS}\right\rangle = \left\langle \pi_1^*\left|\frac{\partial}{\partial Q}\right|d\pi_3\right\rangle \quad (17)$$

By using the expansion in eq 14 and neglecting nonlocal overlap, the integral in eq 17 becomes

$$\left\langle \pi_1^*\left|\frac{\partial}{\partial Q_k}\right|d\pi\right\rangle = a_N\left\langle 2p_N\left|\frac{\partial}{\partial Q_k}\right|d\pi\right\rangle \quad (18)$$

According to eq 16 and 18 the magnitude of β_0 should depend on the square of the weighting coefficient for $2p_N$ in the LCAO approximation for π_1^*. Variations in β_0 with substituent should exist to the degree that they affect a_N.

It is possible to calculate β_0 by using eq 6, the experimental value for k_{nr} in Table IV, and eq 5 to calculate β_0. For the three cases where the calculation can be made, ln $(\beta_0 \times 1s) = 34 \pm 1$. The experimental data are too imprecise to find variations in β_0 if they exist and all three are the same within experimental error.

The MLCT → dd Transition. The nonradiative decay rate constants for the MLCT excited states of four of the five tpm–bpy complexes (X = NH_2, CH_3, H, C_6H_5) are strongly temperature dependent near room temperature. Each of the four is unstable toward photochemically induced loss of pyridine at room temperature (Table II). The odd man out is the lowest energy light

(64) Barigelletti, F.; Juris, A.; Balzani, V.; Belser, A.; von Zelewsky, A. *Inorg. Chem.* **1983**, *22*, 3335.

(65) Buckingham, D. A.; Sargeson, A. M. In *Chelating Agents and Metal Chelates*; Dwyer, F. P., Mellor, D. P., Eds.; Academic: New York, 1964; Chapter 6.

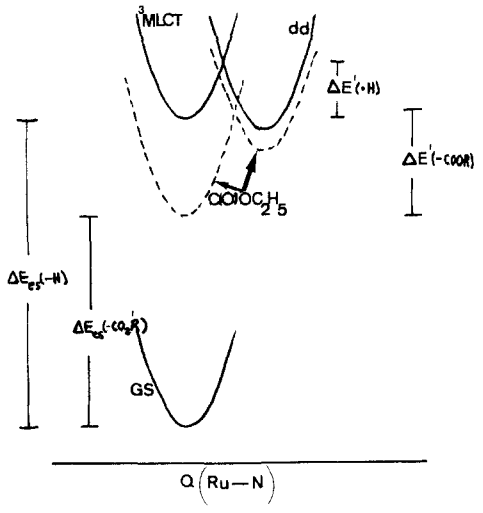

Figure 8. Schematic diagram, showing the differential stabilizing effect of the 4,4′-C(O)OC_2H_5 substituents on the lowest lying MLCT state(s). The coordinate axis has been taken to be a Q(Ru–N) normal mode which is sensitive to the difference in electronic configurations between the MLCT and dd states. The excited-state energies for the X = H (ΔE_{es}(H)) and C(O)OC_2H_5 ($\Delta E_{es}(CO_2R)$ cases were calculated from E_{00} = 16 370 and 14 350, respectively, in 4:1 (v/v) EtOH/MeOH and $\lambda_0 \sim$ 770 and 650 cm^{-1}. Also shown on the diagram are the energies of activation for MLCT → dd surface crossings, $\Delta E'$ = 3000 and ~5100 cm^{-1}. The latter was obtained by linear extrapolation of the $\Delta E'$ values in Table IV to the value of E_{00} = 14 350 cm^{-1} appropriate for the diester complex. The energies of the dd states relative to the MLCT states are unknown.

absorber and emitter, X = C(O)OC_2H_5, where the lifetime is temperature independent and there is no photochemical ligand loss.

In earlier studies, the simultaneous appearance of temperature-dependent lifetimes and photochemical ligand loss has been attributed to a low-lying dd state or states.[3,5-17] The origin of the temperature dependence is in the thermal population of the dd state. Once reached, it either decays to the ground state or undergoes ligand loss. In one kinetic limit, the parameters k^0 and $\Delta E'$, obtained from the temperature dependence of the lifetimes and eq 7, are the preexponential factor and energy of activation for the transition between the MLCT and dd states.[5]

In earlier work on multiple chelates, it was shown that the lowest lying MLCT state(s) could be stabilized relative to the dd states in a coordination environment in which at least one of the three polypyridyl ligands has low-lying π^* levels, e.g., $[Ru(bpy)_2(bpyz)]^{2+}$ (bpyz is 2,2′-bipyrazine), $[Ru(bpy)_2(bpym)]^{2+}$ (bpym is 2,2′-bipyrimidine),[8] $[Ru(bpy)_2(biq)]^{2+}$ (biq is 2,2′-biquinoline),[64] and $[Ru(bpy)(4,4'-(C(O)OC_2H_5)_2\text{-}bpy)_2]^{2+}$.[15] The rationale offered was that the lower π^* levels stabilize the low-lying MLCT states sufficiently that thermal population of the dd states at room temperature is insignificant and that quenches the ligand loss photochemistry.

Passing from electron-donating to electron-withdrawing substituents in the tpm series leads to the stabilization of the MLCT states as shown by the decrease in E_{00} in Figure 6 and Table III. Electronically, the key is the stabilization of the π^*-acceptor orbital in the excited state $(d\pi)^5(\pi^*)^1$ configuration.

Electron-withdrawing substituents should also stabilize the dd states. The electronic configuration of the dd state is $(d\pi)^5(d\sigma^*)^1$ and electron–electron repulsion between the M–N σ bonding electron pair and the excited electron in $d\sigma^*$ will be an important interaction in determining its total energy content. Electron-withdrawing substituents decrease the σ donating ability of the ligands, as shown by pK_a measurements, and should decrease σ based electron–electron repulsion.

From the data in Table III, passing from electron-donating to electron-withdrawing substituents in $[(tpm)Ru(4,4'-(X)_2\text{-}bpy)(py)]^{2+}$ results in an increase in the energy barrier ($\Delta E'$) between the MLCT and dd states from ~2400 to ~4000 cm^{-1}. The data suggest that, as shown schematically in Figure 8, the stabilization of the MLCT states by electron-withdrawing substituents is greater than that for the dd states. From the data in Tables III and IV, $\Delta E'$ increases in a roughly linear fashion with E_{00} as has been observed in earlier studies.[6,7,15] Linear extrapolation of those data to a value of E_{00}(298 K) = 14350 cm^{-1} appropriate for the diester complex gives $\Delta E'(C(O)OC_2H_5) \sim 5100$ cm^{-1}. That barrier is sufficiently high that thermally activated population of low-lying dd states during the MLCT lifetime must be negligible thus explaining the disappearance of ligand loss photochemistry.

MLCT Excited States of Ru. 2,2′-Bipyridine as the Chromophoric Ligand. At the end of this manuscript it seems appropriate to summarize some of the conclusions that can be drawn from our results concerning the role of 2,2′-bipyridine ligands in determining the properties of MLCT chromophores and excited states and of the effect of 4,4′ substituents on that role. (1) Only a single polypyridyl ligand is required to acquire the most important properties of the MLCT excited states. (2) Electron-withdrawing substituents decrease the energies of the π^* acceptor levels to a greater degree than the $d\pi$ donor orbitals. This results in a lowered energy gap between the excited and ground states and lower absorption and emission energies. (3) Changes in the 4,4′ substituents at bpy cause greater bpy-based excited-state distortions than changes in the nonchromophoric ligands. (4) The same pattern of acceptor vibrations is utilized in nonradiative decay by all of the 4,4′ substituted bpy ligands. (5) The vibrationally induced electronic coupling term for nonradiative decay is not profoundly affected by changes in the 4,4′-substituents. (6) Because of a compensation effect between the energy gap and the degree of bpy distortion, the simple energy gap law for nonradiative decay does not apply. (7) With sufficiently good electron-withdrawing substituents, thermally accessible dd states and ligand loss photochemistry can be designed out of the complexes. (8) In terms of synthetic design, chromophoric ligands having low-lying π^* levels offer the advantages of lowered energy light absorptivity and loss of complications from low-lying dd states without a significant loss in excited-state lifetime.

Acknowledgments are made to the Department of Energy under Grant No. DE-FG05-86ER13633 for support of this research. K.B. acknowledges the continuing support of Yarmouk University, Irbid-Jordan. A.L. acknowledges fellowship support for Fulbright "La Caixa" (Barcelona, Spain).

Registry No. $[(tpm)Ru(4,4'-(C(O)OC_2H_5)_2\text{-}bpy)]^{2+}[PF_6]_2^-$, 116663-29-7; $[(tpm)Ru(4,4'-(C_6H_5)_2\text{-}bpy)(py)]^{2+}[Pf_6]_2^-$, 116633-61-5; $[(tpm)Ru(4,4'-(H)_2\text{-}bpy)(py)]^{2+}[PF_6]_2-$, 116633-63-7; $[(tpm)Ru(4,4'-(CH_3)_2\text{-}bpy)(py)]^{2+}[PF_6]_2^-$, 116633-65-9; $[(tpm)Ru(4,4'-(NH_2)_2\text{-}bpy)(py)]^{2+}[PF_6]_2^-$, 116633-67-1.

Supplementary Material Available: Tables of lifetimes as a function of temperature (5 pages). Ordering information is given on any current masthead page.